ARTICLE

BIOTECHNOLOGY and BIOENGINEERING

Helical Spring Template Fabrication of Cell-Laden Microfluidic Hydrogels for Tissue Engineering

Guoyou Huang,[1] Senhao Wang,[1,2] Xiang He,[1] Xiaohui Zhang,[1,2] Tian Jian Lu,[1] Feng Xu[1,2]

[1]Biomedical Engineering and Biomechanics Center, Xi'an Jiaotong University, 28 XianningXi Road, Xi'an 710049, P.R. China; telephone: +86-29-82665937; fax: 86-29-82665937; e-mail: tjlu@mail.xjtu.edu.cn, fengxu@mail.xjtu.edu.cn

[2]The Key Laboratory of Biomedical Information Engineering of Ministry of Education, School of Life Science and Technology, Xi'an Jiaotong University, Xi'an, P.R. China

ABSTRACT: Cell-laden microfluidic hydrogels find great potential applications in microfluidics, tissue engineering, and drug delivery, due to their ability to control mass transport and cell microenvironment. A variety of methods have been developed to fabricate hydrogels with microfluidic channels, such as molding, bioprinting, and photopatterning. However, the relatively simple structure available and the specific equipment required limit their broad applications in tissue engineering. Here, we developed a simple method to fabricate microfluidic hydrogels with helical microchannels based on a helical spring template. Results from both experimental investigation and numerical modeling revealed a significant enhancement on the perfusion ability and cell viability of helical microfluidic hydrogels compared to those with straight microchannels. The feasibility of such a helical spring template method was also demonstrated for microfluidic hydrogels with complex three-dimensional channel networks such as branched helical microchannels. The method presented here could potentially facilitate the development of vascular tissue engineering and cell microenvironment engineering.

Biotechnol. Bioeng. 2013;110: 980–989.

KEYWORDS: microfluidic hydrogels; tissue engineering; helical microchannels; diffusion

No conflict of interest exists in this work.
Correspondence to: T. J. Lu and F. Xu
Contract grant sponsor: National Natural Science Foundation of China
Contract grant number: 10825210
Contract grant sponsor: Major International Joint Research Program of China
Contract grant number: 11120101002
Contract grant sponsor: National 111 Project of China
Contract grant number: B06024
Contract grant sponsor: National Basic Research Program of China
Contract grant number: 2011CB610305
Contract grant sponsor: China Young 1000-Talent Program
Contract grant sponsor: International S&T Cooperation Program of China
Contract grant sponsor: Shaanxi 100-Talent Program
Received 15 June 2012; Revision revised 8 September 2012; Accepted 11 October 2012
Accepted manuscript online 23 October 2012;
Article first published online 12 November 2012 in Wiley Online Library (http://onlinelibrary.wiley.com/doi/10.1002/bit.24764/abstract)
DOI 10.1002/bit.24764

Introduction

With recent development of biomaterials and microengineering methods, hydrogels have attracted increasing interest in biomedical applications, such as microfluidics, biosensors, tissue engineering, and drug delivery (Choi et al., 2007; Cushing and Anseth, 2007; Geckil et al., 2010; Oh et al., 2009; Zhou et al., 2011). This is mostly due to their attractive properties and characteristics including high water content, good biocompatibility, biodegradability, and tunable chemical and physical properties. Despite these advantageous properties, the inefficient solute diffusion within hydrogels restricts their further applications in tissue engineering (Geckil et al., 2010; Wang et al., 2010). Most tissues in vivo are located in regions that are 200–300 μm apart from capillary vascular networks, from which oxygen and nutrient can be obtained and waste products can be removed (Malda et al., 2007; Rouwkema et al., 2008). To address the diffusion limitation, microfluidic hydrogels (i.e., hydrogels embedded with microfluidic channels) have been recently developed to improve mass transfer in hydrogels (Cuchiara et al., 2010; Ling et al., 2007; Xu et al., 2011). The microchannels created within the hydrogels enhanced the delivery of oxygen and nutrients, and the removal of wastes through convective transport by flows perfused through these microchannels.

A variety of methods have been used for microfluidic hydrogel fabrication, including needle- or fiber-based molding (Chrobak et al., 2006), soft lithography (Choi et al., 2007; Golden and Tien, 2007), bioprinting (Lee et al., 2010; Skardal et al., 2010), and photopatterning (Sarig-Nadir et al., 2009; Tsang et al., 2007). Although these methods may hold promise for future applications, several challenges remain for fabricating hydrogels with complicated three-dimensional (3D) microfluidic channels (Huang et al., 2011). For instance, needle- or fiber-embedded molding methods are currently restricted to fabricating microfluidic hydrogels with simple geometry structures (i.e., straight channels). The method of soft lithography is

inherently two-dimensional (2D), requiring cumbersome steps to replicate and assemble into 3D structures. Bioprinting and photopatterning approaches rely on specific hydrogel chemistries and equipment, which may not be available for broad applications. In addition, mechanical extrusion during nozzle-based bioprinting (Xu et al., 2006) and UV (Bryant et al., 2000) or photoinitiators (Williams et al., 2005) used during photopatterning may involve the issue of cell damage for encapsulated cells. Furthermore, some of these methods (e.g., fiber embedded molding method (Madden et al., 2010; Nazhat et al., 2007), omnidirectional printing (Wu et al., 2011), crystal template (Zawko and Schmidt, 2010)) may not be compatible with cell encapsulation. Thus, there is still an unmet need for an alternative method to address these issues, allowing fabricating complicated microfluidic hydrogels to improve perfusion ability and biocompatibility.

The key question is how to maximize mass transport in a limited volume space. To maximize heat transfer, tortuous and repeated heat exchange networks are commonly used in industry, laboratory, and daily life, with increased effective heat exchange area (Linnhoff et al., 1979). In microfluidics, tortuous and repeated microchannel networks are also widely employed to enhance the mixing of different fluids on a single chip (Therriault et al., 2003). As for human body, most of food digestion and absorption take place in small intestine, which naturally coils in lower part of the abdominal cavity, about 7 m in extent, with its inner surface bestrewed by circular folds and villi (Tortora and Derrickson, 2008). Inspired by these natural observations and engineering applications, we developed a simple helical spring template method to fabricate microfluidic hydrogels with helical microchannels. We characterized the perfusion ability of the helical microchannels both experimentally and numerically. We evaluated cell viability post-encapsulation and after perfusion culture for microfluidic hydrogels with helical microchannels, and compared to those with straight microchannels. We also applied this method to fabricate microfluidic hydrogels with branched and intercross helical microchannels, as well as combined helical and straight microchannels.

Materials and Methods

Fabrication of Microfluidic Hydrogels

In this study, we used 2% agarose hydrogel embedded with fibroblasts as a cell-laden hydrogel model system for general study. We used agarose to fabricate hydrogels due to its proved biocompatibility and wide application for cell encapsulation (Bian et al., 2009; Park et al., 2010). Low-gelling temperature agarose powder (type VII-A, Sigma-Aldrich, Saint Louis, MO) was dissolved in deionized water (DI) at 70°C at a concentration of 2% (w/v), with which the compressive modulus (~76 kPa (Huang et al., 2012)) is on the range of some native soft tissues such as skin and cartilage (Bian et al., 2009; McKee et al., 2011). The agarose solution was cooled down to 40°C and injected into a poly(methyl methacrylate) (PMMA) chamber, which was cut by using a laser etcher (Universal VLS 2.30, USA). The inner dimension of the chamber is 24 mm × 12 mm × 5 mm, with a hole of 2.5 mm diameter on each side (Fig. 1a). A helical symmetric stainless spring, with wire diameter (WD) of 300 μm, outer diameter (OD) of 2.5 mm, and pitch gauge (PG) of 2 mm (i.e., WD × OD × PG = 300 μm × 2.5 mm × 2 mm), was inserted from the center hole of a side-wall, the opposite center hole was plugged by a luer adapter with inner diameter (ID) of 1.6 mm. The two side holes were fitted with two luer adapters and with microneedles (OD = 1.6 mm) through insertion, serving as inlet and outlet after removing the microneedles. The entire casting mold with hot agarose solution was placed at 4°C for 20 min to form agarose hydrogels. The helical spring was subsequently circumrotated out to form helical microchannels in hydrogels. The remaining center hole was plugged with a luer adapter. After aspirating out remaining water from the helical microchannels, the microfluidic hydrogels were imaged using an inverted fluorescent microscope in bright-field mode (Olympus IX-81, Tokyo, Japan). To fabricate microfluidic hydrogels with different sizes of helical microchannels, helical springs with WD × OD × PG = 300 μm × 2.5 mm × 1 mm, 500 μm × 3 mm × 2.7 mm, and 500 μm × 3 mm × 1.6 mm were also used.

Microfluidic hydrogels with straight microchannels were also fabricated as controls, including diameters of 300 μm (i.e., the same wire diameter as helical spring with WD = 300 μm) and 600 μm (at this diameter, the straight microchannel would occupy the same volume in the engineered microfluidic hydrogel construct as that occupied by a helical spring with WD × OD × PG = 300 μm × 2.5 mm × 2 mm, that is, the same porosity).

Diffusion Characterization

To characterize the diffusion property of the fabricated microfluidic hydrogels, the microneedles inserted through the luer fittings were removed and the luer fittings were connected to silicon tubes (Fig. 1b). Rhodamine B solution (RhB, Mw 479.01, Sigma) with the concentration of 5 μM was pumped into and filled the microchannels in hydrogels instantaneously. Fluorescent microscope (Olympus IX-81) was used to capture fluorescent images at different time points (1, 5, 10, 20, and 40 min). NIH software ImageJ was used to quantify fluorescence intensities, which were normalized to the corresponding maximal fluorescence intensity at each time point, respectively. Spatiotemporal diffusion profiles of RhB in microfluidic hydrogels at different time points were plotted in the format of fluorescent intensities versus the distance from the center of the microfluidic hydrogel. The fluorescence intensity profiles for microfluidic hydrogels with helical microchannels were averaged from 2 mm length along the

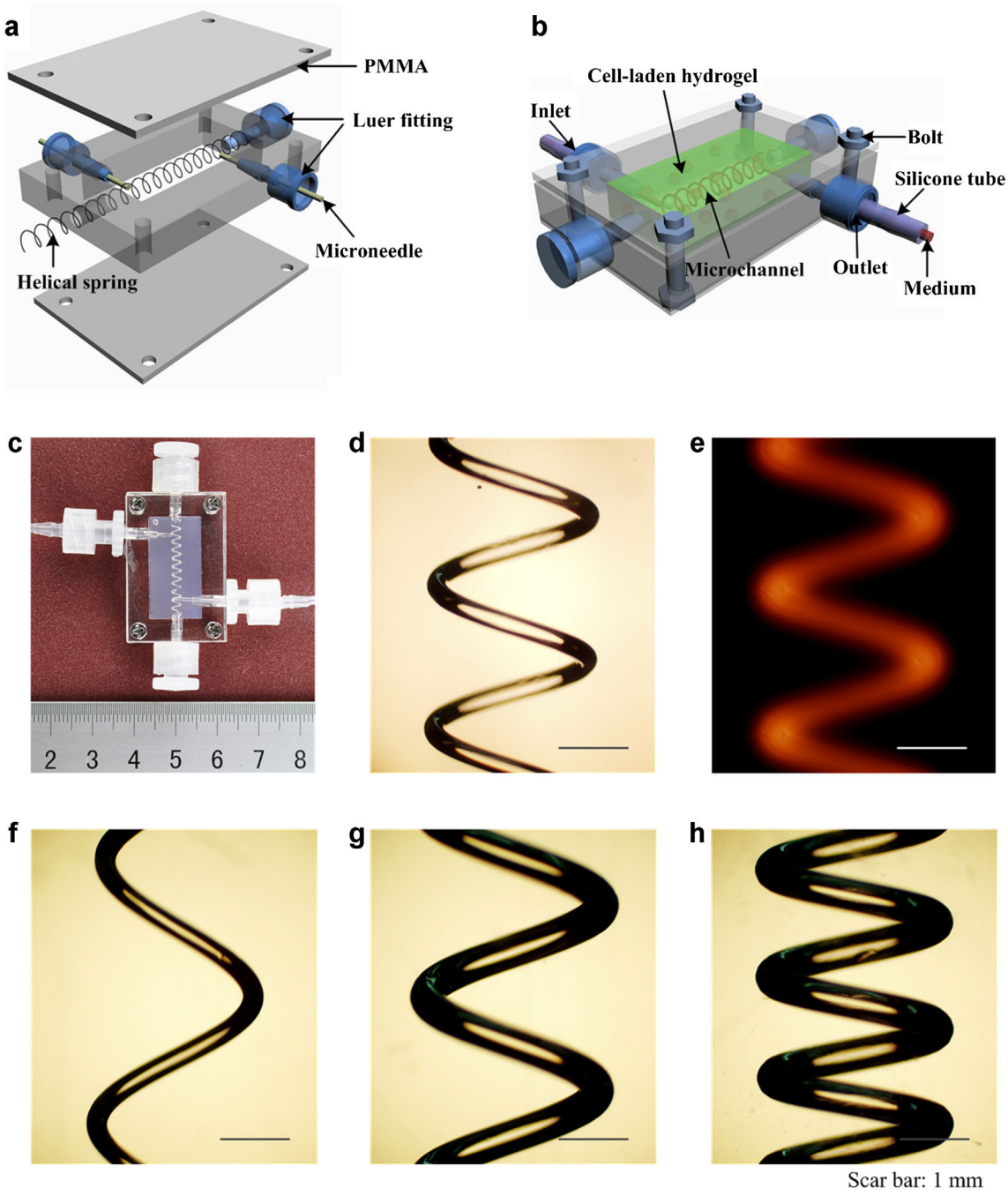

Figure 1. Fabrication of microfluidic hydrogels based on helical spring template. **a**: Purpose-built PMMA system before assembling. The medial PMMA chamber and the two cover plates were cut by using a laser etcher. The inner dimension of the chamber is 24 mm × 12 mm × 5 mm, with a hole on each side wall. A helical spring was inserted from the center hole of a side-wall, and the opposite center hole was plugged by a luer adapter. The two side holes were fitted with two luer adapters and with the inserted microneedles. **b**: After assembling and gelling hydrogels, the helical spring and microneedles were removed, leaving behind helical channels and hydrogel inlet/outlet, respectively. Silicone tubes were then connected to the inlet and outlet for medium perfusion. **c**: Actual picture of microfluidic hydrogel in PMMA device for perfusion. **d**: Bright field image of helical microchannel (WD × OD × PG = 300 μm × 2.5 mm × 2 mm) in hydrogel after removing helical spring and aspirating out remaining water in microchannels. **e**: Fluorescence image of (d) with helical microchannel filled by 5 μM RhB solution. **f–h**: Bright field image of helical microchannels with different sizes in hydrogels after removing helical spring and aspirating out remaining water in microchannels: (f) WD × OD × PG = 300 μm × 2.5 mm × 1 mm, (g) WD × OD × PG = 500 μm × 3 mm × 2.7 mm, and (h) WD × OD × PG = 500 μm × 3 mm × 1.6 mm.

channel (i.e., one pitch gauge of helical microchannel, as dashed yellow line in Fig. 2g), considering non-uniform profile along the channel length direction and rotational symmetry of the helical microchannels.

Numerical Modeling of Oxygen Transport in Microfluidic Hydrogels

To numerically study the perfusion ability of the microfluidic hydrogels, we modeled oxygen delivery and utilization by cells, mainly because oxygen has low water solubility (~0.125 mM at 1 atmospheric pressure) and is highly consumed by cells (Guaccio et al., 2008; House et al., 2011; Nikolaev et al., 2010). The cell-laden hydrogel region is denoted by Ω_h, the microchannel region is denoted by Ω_c, and the microchannel wall (i.e., the interface between Ω_h and Ω_c) is denoted by Γ.

The medium flow in microchannel can be described by incompressible Navier–Stokes equation:

$$\rho_0\left(\frac{\partial u}{\partial t}+(u\cdot\nabla)u\right)=-\nabla p+\mu\nabla^2 u,\ \text{in}\ \Omega_c \tag{1}$$

$$\nabla\cdot u=0,\ \text{in}\ \Omega_c \tag{2}$$

where $\mathbf{u}=(u,v,w)$ is the flow velocity, p is pressure, ρ_0 is the medium density, and μ is the medium viscosity.

Oxygen transport in microchannel can be described by convective-diffusion equation:

$$\frac{\partial c}{\partial t}+u\cdot\nabla c=D_0\nabla^2 c,\ \text{in}\ \Omega_c \tag{3}$$

Here, c represents the oxygen concentration, D_0 is the diffusion coefficient of oxygen in medium. For oxygen transport in cell-laden hydrogel, the following equation is derived by applying porous medium theory (Nicholson, 2001; Nicholson and Phillips, 1981) and average theorem (Gray and Lee, 1977) to Fick's law:

$$\alpha\frac{\partial c}{\partial t}=D^*\nabla^2 c-\frac{V_{max}c}{K_m+c}\rho,\ \text{in}\ \Omega_h \tag{4}$$

where, α is the volume fraction of the extracellular space (i.e., the volume of hydrogels without cells), D^* is the effective or apparent (scalar) diffusion coefficient of oxygen in cell-laden hydrogel, V_{max} is the maximum uptake velocity of oxygen by cells, K_m is the concentration at which the half-maximum rate occurs, and ρ is the cell density in hydrogel.

The last term in Equation (4) represents Michaelis–Menten description of the saturated oxygen uptake rate by cells per unit volume (Nicholson, 1995; Sengers et al., 2005). Thus, the integration of this term over Ω_h gives oxygen consumption rate by cells in hydrogel constructs, as:

$$Q=\int_{\Omega_h}\frac{V_{max}c\rho}{K_m+c}dV \tag{5}$$

The oxygen concentration in the inlet was set as a constant, that is, 0.125 mM, which reflects oxygen concentration in air-equilibrated buffer solution (Nikolaev et al., 2010; Obradovic et al., 2000; Vandegriff and Olson, 1984). No slip boundary condition for flow velocity was applied on Γ. For the other outmost boundaries of the construct, no flux boundary condition was used. The medium was perfused through the microchannel at a constant volumetric flow rate of 5 μL/min. The initial value for oxygen concentration in cell-laden microfluidic hydrogels was set at 0 mM. Other typical parameters were chosen following the references (Lightfoot and Duca, 2000; Nikolaev et al., 2010; Obradovic et al., 2000; Sengers et al., 2005; Sucosky et al., 2004; Williams et al., 2002), Table I. The simulation was conducted using COMSOL Multiphysics V4.2 (COMSOL, Stockholm, Sweden).

Cell Encapsulation and Cell Viability Evaluation

We used NIH 3T3 cell line in this study, which is commonly used to evaluate cell viability under perfusion culture of cell-laden microfluidic hydrogels (Cuchiara et al., 2010; Golden and Tien, 2007; Lee et al., 2010; Song et al., 2009). The cell line was purchased from the Cell Bank of the Chinese Academy of Sciences (Shanghai, China) and incubated at 37°C with 5% CO_2. Dulbecco's modified Eagle's medium (DMEM, high glucose), supplemented with 10% fetal bovine serum (FBS) and 1% penicillin–streptomycin mixture (Gibco-BRL), was used to culture 3T3 cells. 3T3 cells were digested from culture plates and centrifuged, and then suspended with fresh culture medium at the concentration of 1.5×10^7 cells/mL before use.

To encapsulate cells, agarose solution with a concentration of 3% (w/v) was prepared and autoclaved, and mixed with cell suspension at the volume ratio of 2:1 v/v at 40°C. Cell-laden microfluidic hydrogels were prepared using the same procedures as described above for the fabrication of cell-free microfluidic hydrogel constructs.

For perfusion culture of cell-laden microfluidic hydrogels, culture medium was flowed through the microchannels in hydrogels at a rate of 5 μL/min with a syringe pump (LSP02-1B, Baoding, Hebei, China) working on a withdraw mode. To evaluate cell viability, disk-shaped hydrogel samples of ~1 mm thick were prepared using a razor blade from cell-laden microfluidic hydrogels post-fabrication and perfusion culture. The samples were incubated in Live/Dead solution (Molecular Probes, Eugene, OR) at 37°C for 30 min. The stained slices were then visualized under a fluorescence microscope. The number of live and dead cells was counted by using ImageJ.

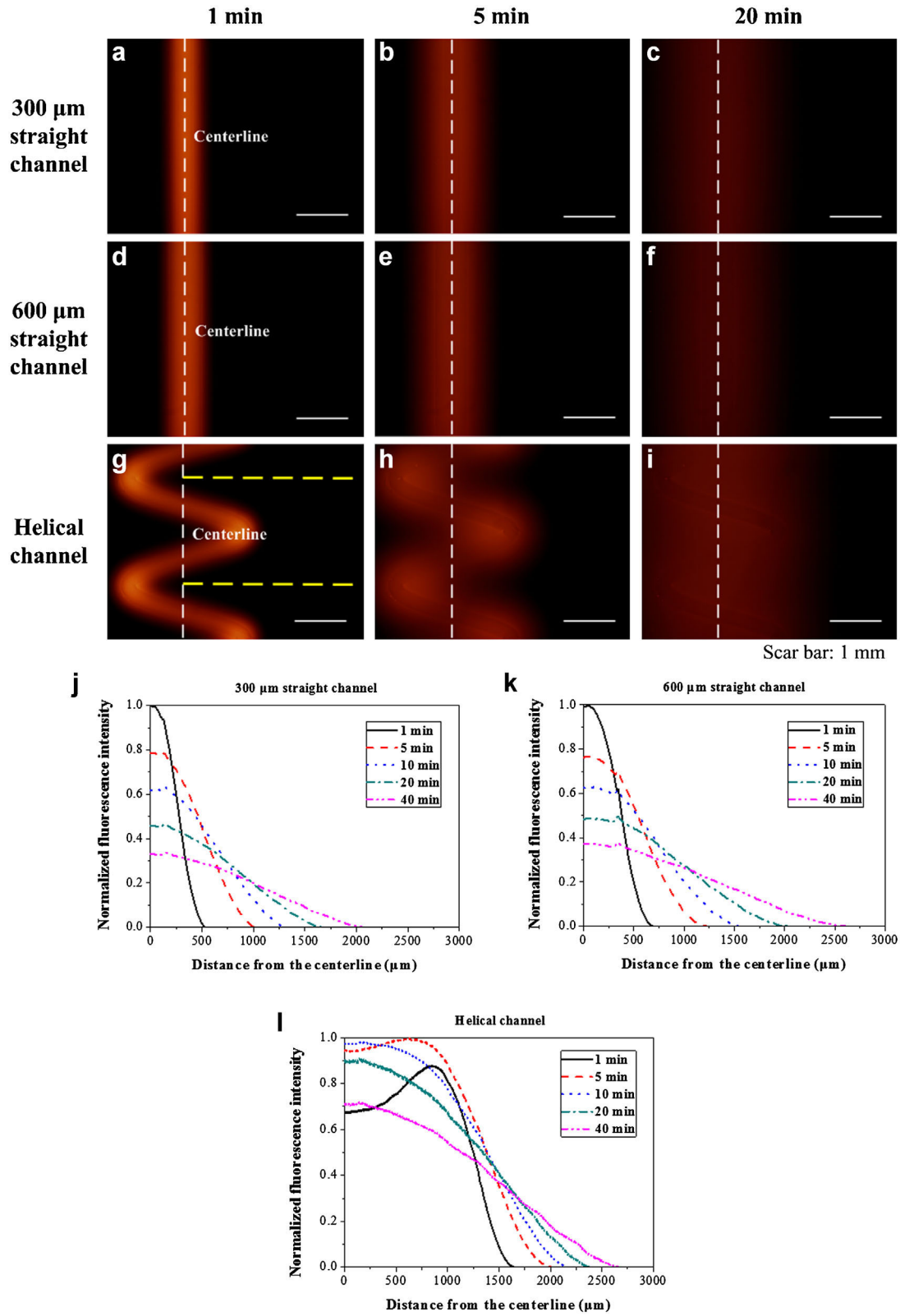

Figure 2. Diffusion of RhB in microfluidic hydrogels. **a–i**: Sequential fluorescence images of RhB diffused out from 300 µm straight microchannels (a–c), 600 µm straight microchannels (d–f), and helical microchannels (WD × OD × PG = 300 µm × 2.5 mm × 2 mm; g–i), respectively. The white dashed lines indicated centerlines of the hydrogels. **j–l**: Plots of normalized fluorescence intensity versus distance from hydrogel centerline at sequential time points after instantaneously pumping and filling RhB at 5 µM concentration.

Table I. Parameters used for modeling.

Names	Denotations	Values	Refs.
Medium density	ρ_0	$1\ g/cm^3$	Sucosky et al. (2004) and
Medium viscosity	μ	10^{-2} g/cm/s	Williams et al. (2002)
Oxygen diffusion coefficient in medium	D_0	$3 \times 10^{-5}\ cm^2/s$	Lightfoot and Duca (2000)
Effective oxygen diffusion coefficient in cell-laden hydrogel	D^*	$1.5 \times 10^{-5}\ cm^2/s$	Nikolaev et al. (2010) and
Maximum uptake velocity of oxygen by cells in hydrogel	V_{max}	1.86×10^{-18} mol/cell/s	Obradovic et al. (2000)
Michaelis–Menten constant	K_m	6×10^{-3} mM	
Volume fraction of the extracellular space	α	0.96	Sengers et al. (2005)
Initial cell density in hydrogel	ρ	$5 \times 10^6\ cell/cm^3$	—

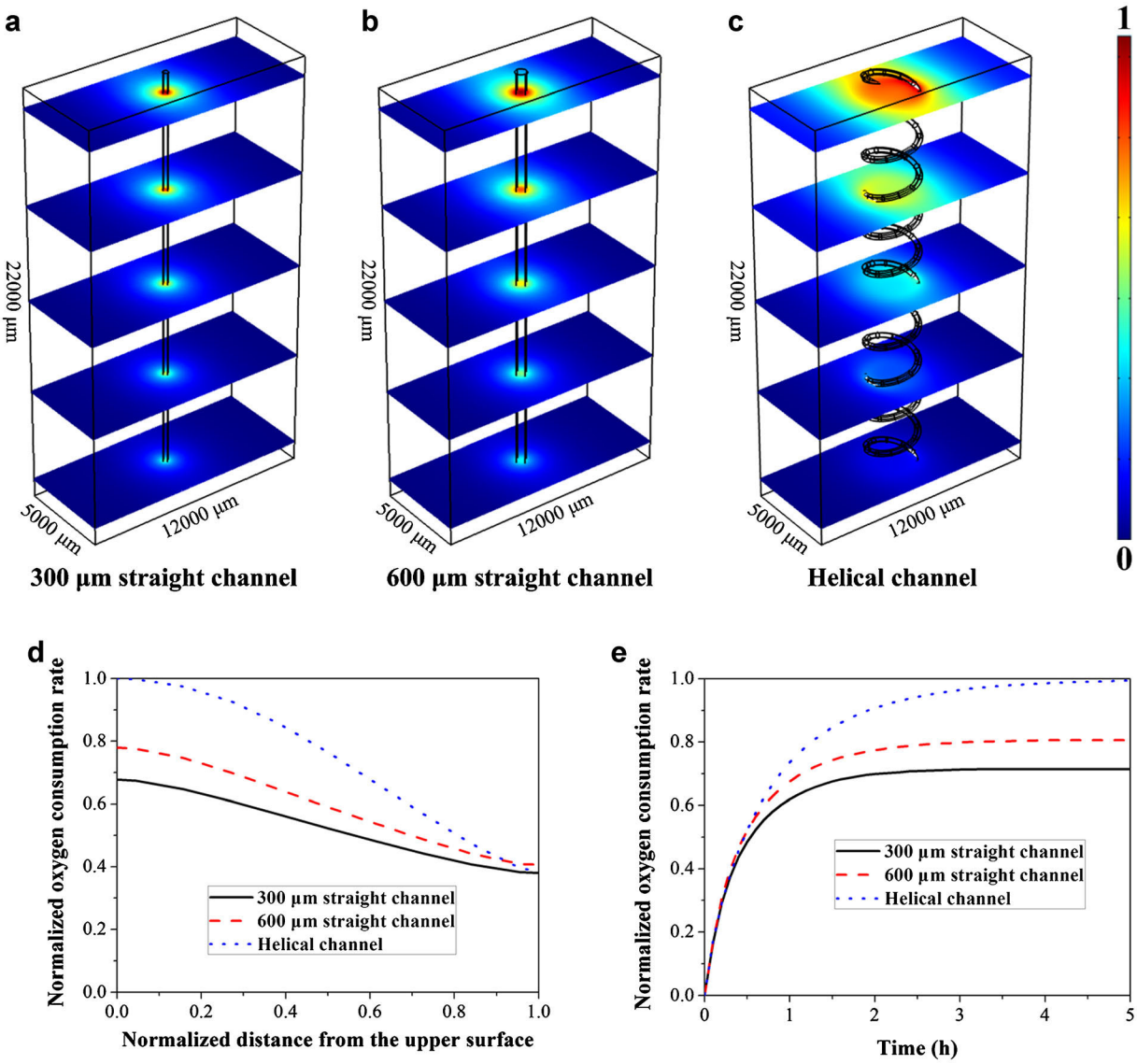

Figure 3. Simulation of oxygen transport and consumption by cells. **a–c**, simulation results of normalized oxygen concentration distribution at different slices from upper inlet surface down to outlet surface with (a) 300 μm straight microchannels, (b) 600 μm straight microchannels, and (c) helical microchannels (WD × OD × PG = 300 μm × 2.5 mm × 2 mm), respectively. **d**: Plots of normalized oxygen consumption rate in slices as a function of the distance from the upper inlet surface. **e**: Evolvement of normalized oxygen consumption rate for the entire constructs.

Demonstration for Fabricating Microfluidic Hydrogels With Complex Microchannels

Helical springs and microneedles were assembled into complex structures as indicated in Figure 5a–c. Specialized PMMA chambers were customized to hold these structures. The fabrication process was the same as described in Fabrication of Microfluidic Hydrogels Section. A stereomicroscope (Leica M125, Milton Keynes, UK) equipped with a ToupTek UHCCD05100KPA CCD camera was employed to capture the microchannel networks in hydrogels using a relative wider visual angle compared to Olympus IX-81.

Statistical Analysis

Error bars for cell viability evaluation represent standard deviation ($n = 3$). Paired t-test was used to analyze statistically significant difference, with the threshold set at 0.05 ($P < 0.05$).

Results and Discussion

The engineered microfluidic hydrogel connected to a flow loop in a PMMA chamber is illustrated in Figure 1c. The structure of the helical microchannels (WD × OD × PG = 300 μm × 2.5 mm × 2 mm) within hydrogels is clearly observed in a bright field image (Fig. 1d). To further verify their interconnectivity, RhB was pumped through microfluidic hydrogels instantaneously and immediately visualized under fluorescence microscope (Fig. 1e). The existence of 3D helical microchannels in hydrogels and their interconnectivity for perfusion was observed. Hydrogels with helical microchannels of WD × OD × PG = 300 μm × 2.5 mm × 1 mm (Fig. 1f), 500 μm × 3 mm × 2.7 mm (Fig. 1g), and 500 μm × 3 mm × 1.6 mm (Fig. 1h), respectively, were also fabricated, with other sizes of helical microchannels available by simply adjusting the corresponding parameters of helical springs.

To evaluate the mass transport ability of hydrogels with helical microchannels, spatial distribution of RhB was characterized at selected time points. The results indicated that RhB diffused out from the microchannels into the surrounding hydrogel (Fig. 2a–i). RhB diffused and reached a larger area range in the sense of volume (out from the microchannels) in microfluidic hydrogels with helical microchannels (WD × OD × PG = 300 μm × 2.5 mm × 2 mm; Fig. 2i) than those with 300 μm (Fig. 2c) and 600 μm straight microchannels (Fig. 2f). This was obviously observed from normalized fluorescence intensity profiles, see Figure 2j–l.

To study the influence of microchannel structure upon oxygen delivery, oxygen transport and its consumption by cells in hydrogels were modeled numerically. Based on normalized oxygen concentration distribution (Fig. 3a and b), we observed that oxygen concentration in cell-laden hydrogels increased when the straight channel diameter increased from 300 to 600 μm. However, this improvement was rather limited and the decrease of cell-hydrogel space along with the increase of channel diameter should be also considered. As shown in Figure 3c–e, helical microchannels allow much more effective oxygen transport in cell-laden hydrogels and the delivery of oxygen to cells than straight microchannels. This is due to the fact that the interface area that oxygen diffused out from the microchannels into cell-laden hydrogels is much larger for helical microchannels than that for straight microchannels with the same channel diameter or channel volume. For instance, the interface area is ~7.50 mm^2 for one cycle length of helical microchannel with WD × OD × PG = 300 μm × 2.5 mm × 2 mm, while it is only 1.88 mm^2 for 2 mm length of 300 μm straight

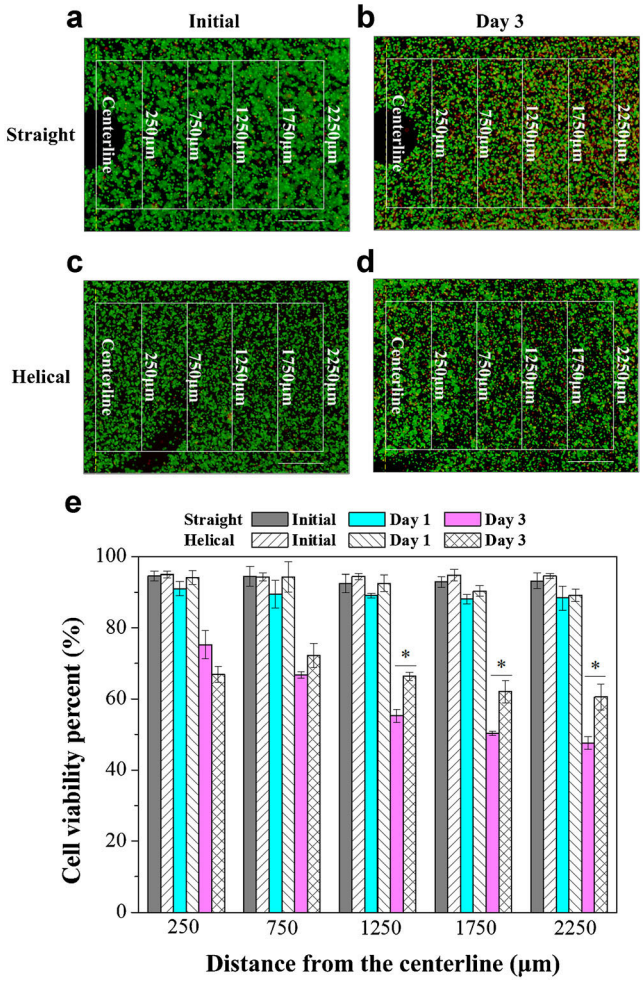

Figure 4. Cell viability in hydrogels post-encapsulation and under perfusion culture. **a–d**: Fluorescent images of stained live (green) and dead (red) cells for (a and b) cell-laden hydrogels with 600 μm straight microchannels and (c and d) helical microchannels (WD × OD × PG = 300 μm × 2.5 mm × 2 mm) (a, c) post-fabrication and (b and d) after 3 days perfusion culture, respectively. The perfusion rate was 5 μL/min. **e**: Cell viability as a function of distance from hydrogel centerline as indicated in (a–d). (*) indicates significant difference between cell-laden hydrogels with straight microchannels and those with helical microchannels after 3 days perfusion culture (paired t-test, $n = 3$, $P < 0.05$).

microchannel and 3.77 mm^2 for 2 mm length of 600 μm straight microchannel.

To further verify the superior perfusion ability of helical microchannels (with WD× OD×PG =300 μm2.5mm×2mm) in cell-laden hydrogels, cell viability post-encapsulation and after perfusion culture was evaluated and compared to those within hydrogels with 600 μm straight microchannels (the same porosity as that of hydrogels with helical microchannels), see Figure 4. Cell viability was quantified from five regions (with identical sizes) as a function of distance from the centerlines as indicated in Figure 4a–d. It was shown that more than 94% of 3T3 cells remained alive post-fabrication process, and more than 89% of cells remained alive after 1 day in perfusion culture. The distribution of cell viability was uniform and no significant difference (paired t-test, $n = 3$, $P < 0.05$) between cell-laden hydrogels with straight microchannels and those with helical microchannels was observed, Figure 4e. However, after perfusion culture for 3 days, the viability of cells in cell-laden hydrogels with straight microchannels decreased out from the centerlines. In contrast, significantly increased cell viability was observed for out regions (750 μm outside from the centerlines) of cell-laden hydrogels with helical microchannels than those with straight microchannels, Figure 4e. These results demonstrate the enhanced perfusion ability of helical channels for cell-laden hydrogels. Due to partially unavailable parameters of our cell-laden hydrogel and perfusion culture system, we did not intend to fully relate the experimental results to those observed from numerical modeling. However, both the numerical and experimental results indicate the enhanced perfusion ability of microfluidic hydrogels with helical microchannels. The conclusion may be extended to other microfluidic cell-laden hydrogel systems.

Vascular systems are composed of hierarchically branched microchannel networks. However, existing methods are either limited to hydrogel fabrication with simple channel structures (e.g., needle embedded molding method (Chrobak et al., 2006)) or technically expensive and cumbersome to use methods (e.g., soft lithography (Choi et al., 2007; Golden and Tien, 2007), photopatterning (Sarig-Nadir et al., 2009; Tsang et al., 2007)). In addition, some methods may also involve biocompatibility issues due to the use of organic solvent (e.g., fiber embedded method (Madden et al., 2010; Nazhat et al., 2007)) or incompatible operation conditions (e.g., crystal template (Zawko and Schmidt, 2010)). Inspired from natural heat exchange systems and microfluidic mixing technologies, we developed a simple method to fabricate microfluidic hydrogels with helical microchannels based on helical springs. The helical springs can be gently circumrotated out to leave helical microchannels in hydrogels without significant effect on structure-fidelity. Compared to hydrogels with straight microchannels at the same diameter or porosity, hydrogels with helical microchannels possess much more effective mass exchange area (equivalently, specific surface area or

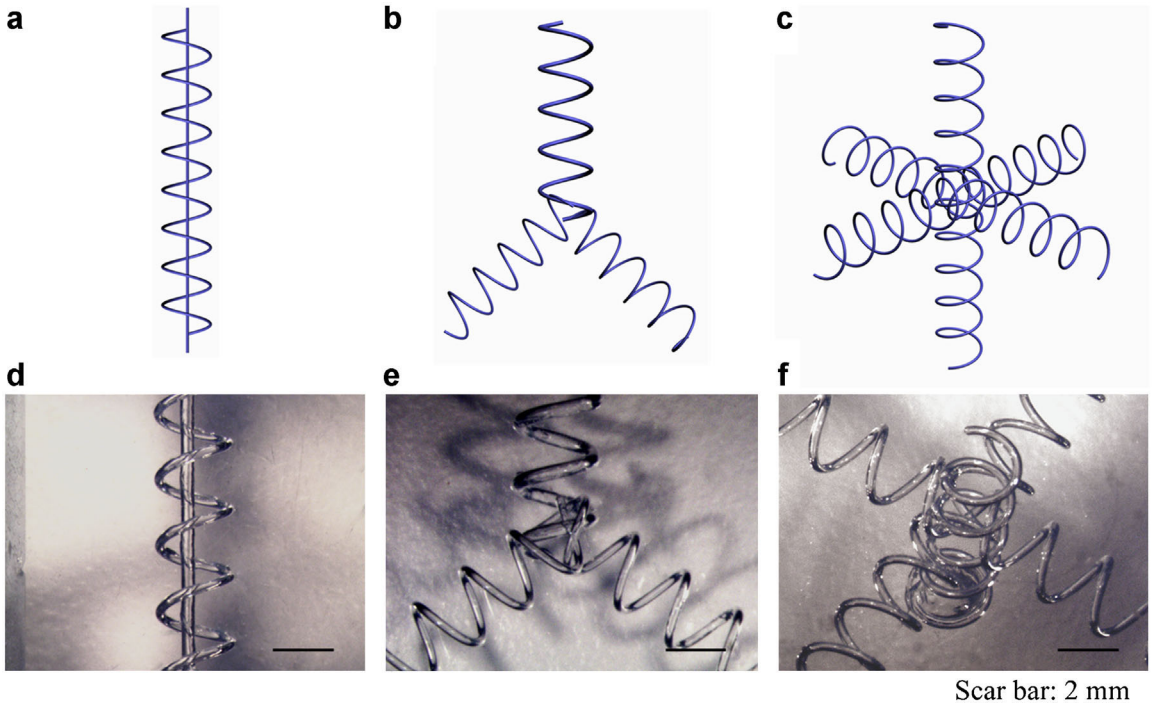

Figure 5. Proposed fabrication scheme for hydrogels with complex microchannels. **a**–**c**: Schematic representation of microchannel networks with (a) combination of helical and straight microchannels, (b) branching, and (c) intercross structures with helical microchannels. **d**–**f**: Corresponding microchannels in hydrogels were visualized by stereomicroscope after removing templates (i.e., microneedle and helical spring) and aspirating out remaining water in microchannels.

surface area per unit volume). For example, the effective mass exchange area for helical microchannel with WD × OD × PG = 300 μm × 2.5 mm × 2 mm is about twice as that of 600 μm straight microchannel (i.e., the same porosity) and fourfold as that of 300 μm straight microchannel (i.e., the same diameter). The effective mass exchange area is associated with the perfusion ability of microfluidic hydrogels, and can be further improved by increasing OD and PG of the helical microchannels. In addition to combining helical microchannels with straight microchannels, helical microchannels with branched and intercross microchannel networks can also be easily fabricated (e.g., Fig. 5). One possible issue is the influence of shear stress resulting from helical microfluidic flows upon the mechanical stability of hydrogel constructs, especially on vascular stability and functional performance when the helical microchannels are endothelialized. Another issue is the lack of cell adhesion to agarose, which may influence the ability of cells to spread and migrate. One possible solution is to add adhesion cues (e.g., laminin, fibronectin) into agarose precursor solution or by using bioactive hydrogels such as bioactive modified poly(ethylene glycol) hydrogels (Zhu, 2010). These will be studied in our future work.

Conclusions

Microfluidic hydrogels enable effective deliveries of oxygen, nutrient and grow factors to, as well as removal of waste from encapsulated cells, thus hold great promise for the fabrication of large tissue constructs, which has been a challenge for mini-culture methods such as spotted arrays. Here, we developed a templating method to fabricate microfluidic hydrogels with helical microchannels. Different channel geometries were characterized based on the diffusion of small molecules from a channel into a hydrogel through experiments and numerical simulation. The helical microchannels in the fabricated hydrogels showed improved perfusion ability and enhanced delivery of oxygen and nutrients to cells in hydrogels compared to straight microchannels. The method developed here is simple and extendable, and does not require any sophisticated and costly equipment, making it attractive and broadly applicable for microfluidics and tissue engineering.

F.X. was also partially supported by the China Young 1000-Talent Program and Shaanxi 100-Talent Program.

References

Bian L, Angione SL, Ng KW, Lima EG, Williams DY, Mao DQ, Ateshian GA, Hung CT. 2009. Influence of decreasing nutrient path length on the development of engineered cartilage. Osteoarthritis Cartilage 17(5): 677–685.

Bryant SJ, Nuttelman CR, Anseth KS. 2000. Cytocompatibility of UV and visible light photoinitiating systems on cultured NIH/3T3 fibroblasts in vitro. J Biomater Sci Polym Ed 11(5):439–457.

Choi NW, Cabodi M, Held B, Gleghorn JP, Bonassar LJ, Stroock AD. 2007. Microfluidic scaffolds for tissue engineering. Nat Mater 6(11):908–915.

Chrobak KM, Potter DR, Tien J. 2006. Formation of perfused, functional microvascular tubes in vitro. Microvasc Res 71(3):185–196.

Cuchiara MP, Allen AC, Chen TM, Miller JS, West JL. 2010. Multilayer microfluidic PEGDA hydrogels. Biomaterials 31(21):5491–5497.

Cushing MC, Anseth KS. 2007. Hydrogel cell cultures. Science 316(5828): 1133–1134.

Geckil H, Xu F, Zhang XH, Moon S, Utkan Demirci U. 2010. Engineering hydrogels as extracellular matrix mimics. Nanomedicine 5(3):469–484.

Golden AP, Tien J. 2007. Fabrication of microfluidic hydrogels using molded gelatin as a sacrificial element. Lab Chip 7(6):720–725.

Gray W, Lee P. 1977. On the theorems for local volume averaging of multiphase systems. Int J Multiphase Flow 3:333–340.

Guaccio A, Borselli C, Oliviero O, Netti PA. 2008. Oxygen consumption of chondrocytes in agarose and collagen gels: A comparative analysis. Biomaterials 29(10):1484–1493.

House M, Daniel J, Elstad K, Socrate S, Kaplan DL. 2011. Oxygen tension and formation of cervical-like tissue in two-dimensional and three-dimensional culture. Tissue Eng A 18(5–6):499–507.

Huang GY, Zhou LH, Zhang QC, Chen YM, Sun W, Xu F, Lu TJ. 2011. Microfluidic hydrogels for tissue engineering. Biofabrication 3(1): 012001.

Huang G, Zhang X, Xiao Z, Zhang Q, Zhou J, Xu F, Lu TJ. 2012. Cell-encapsulating microfluidic hydrogels with enhanced mechanical stability. Soft Matter 8(41):10687–10694.

Lee W, Lee V, Polio S, Keegan P, Lee JH, Fischer K, Park JK, Yoo SS. 2010. On-demand three-dimensional freeform fabrication of multi-layered hydrogel scaffold with fluidic channels. Biotechnol Bioeng 105(6): 1178–1186.

Lightfoot EN, Duca KA, editors. 2000. The role of mass transfer in tissue function. London: CRC Press.

Ling Y, Rubin J, Deng Y, Huang C, Demirci U, Karp JM, Khademhosseini A. 2007. A cell-laden microfluidic hydrogel. Lab Chip 7(6):756–762.

Linnhoff B, Mason DR, Wardle I. 1979. Understanding heat-exchanger networks. Comput Chem Eng 3(1–4):295–302.

Madden L, Mortisen D, Sussman E, Dupras S, Fugate J, Cuy J, Hauch K, Laflamme M, Murry C, Ratner B. 2010. Proangiogenic scaffolds as functional templates for cardiac tissue engineering. Proc Natl Acad Sci USA 107(34):15211.

Malda J, Klein TJ, Upton Z. 2007. The roles of hypoxia in the in vitro engineering of tissues. Tissue Eng 13(9):2153–2162.

McKee CT, Last JA, Russell P, Murphy CJ. 2011. Indentation versus tensile measurements of Young's modulus for soft biological tissues. Tissue Eng B Rev 17(3):155–164.

Nazhat SN, Abou Neel EA, Kidane A, Ahmed I, Hope C, Kershaw M, Lee PD, Stride E, Saffari N, Knowles JC, Brown RA. 2007. Controlled microchannelling in dense collagen scaffolds by soluble phosphate glass fibers. Biomacromolecules 8(2):543–551.

Nicholson C. 1995. Interaction between diffusioin and Michaelis-Menten uptake of dopamine after iontophoresis in striatum. Biophys J 68(5): 1699–1715.

Nicholson C. 2001. Diffusion and related transport mechanisms in brain tissue. Rep Prog Phys 64(7):815–884.

Nicholson C, Phillips JM. 1981. Ion diffusion modified by tortuosity and volume fraction in the extracellular micro-environment of the rat cerebellum. J Physiol Lond 321(Dec):225–257.

Nikolaev NI, Obradovic B, Versteeg HK, Lemon G, Williams DJ. 2010. A validated model of GAG deposition, cell distribution, and growth of tissue engineered cartilage cultured in a rotating bioreactor. Biotechnol Bioeng 105(4):842–853.

Obradovic B, Meldon JH, Freed LE, Vunjak-Novakovic G. 2000. Glycosaminoglycan deposition in engineered cartilage: Experiments and mathematical model. Aiche J 46(9):1860–1871.

Oh JK, Lee DI, Park JM. 2009. Biopolymer-based microgels/nanogels for drug delivery applications. Progr Polym Sci 34(12):1261–1282.

Park JH, Chung BG, Lee WG, Kim J, Brigham MD, Shim J, Lee S, Hwang CM, Durmus NG, Demirci U, Khademhosseini A. 2010. Microporous

cell-laden hydrogels for engineered tissue constructs. Biotechnol Bioeng 106(1):138–148.
Rouwkema J, Rivron NC, van Blitterswijk CA. 2008. Vascularization in tissue engineering. Trends Biotechnol 26(8):434–441.
Sarig-Nadir O, Livnat N, Zajdman R, Shoham S, Seliktar D. 2009. Laser photoablation of guidance microchannels into hydrogels directs cell growth in three dimensions. Biophys J 96(11):4743–4752.
Sengers BG, Heywood HK, Lee DA, Oomens CWJ, Bader DL. 2005. Nutrient utilization by bovine articular chondrocytes: A combined experimental and theoretical approach. J Biomech Eng Trans Asme 127(5):758–766.
Skardal A, Zhang J, Prestwich G. 2010. Bioprinting vessel-like constructs using hyaluronan hydrogels crosslinked with tetrahedral polyethylene glycol tetracrylates. Biomaterials 31(24):6173–6181.
Song YS, Lin RL, Montesano G, Durmus NG, Lee G, Yoo SS, Kayaalp E, Haeggstrom E, Khademhosseini A, Demirci U. 2009. Engineered 3D tissue models for cell-laden microfluidic channels. Anal Bioanal Chem 395(1):185–193.
Sucosky P, Osorio DF, Brown JB, Neitzel GP. 2004. Fluid mechanics of a spinner-flask bioreactor. Biotechnol Bioeng 85(1):34–46.
Therriault D, White SR, Lewis JA. 2003. Chaotic mixing in three-dimensional microvascular networks fabricated by direct-write assembly. Nat Mater 2(4):265–271.
Tortora GJ, Derrickson BH. 2008. Principles of anatomy and physiology. New York: John Wiley & Sons.
Tsang VL, Chen AA, Cho LM, Jadin KD, Sah RL, DeLong S, West JL, Bhatia SN. 2007. Fabrication of 3D hepatic tissues by additive photopatterning of cellular hydrogels. Faseb J 21(3):790–801.
Vandegriff KD, Olson JS. 1984. Morphological and physiological factors affecting oxygen-uptake and release by red-blood-cells. J Biol Chem 259(20):2619–2627.
Wang XH, Yan YN, Zhang RJ. 2010. Recent trends and challenges in complex organ manufacturing. Tissue Eng B Rev 16(2):189–197.
Williams KA, Saini S, Wick TM. 2002. Computational fluid dynamics modeling of steady-state momentum and mass transport in a bioreactor for cartilage tissue engineering. Biotechnol Progr 18(5):951–963.
Williams CG, Malik AN, Kim TK, Manson PN, Elisseeff JH. 2005. Variable cytocompatibility of six cell lines with photoinitiators used for polymerizing hydrogels and cell encapsulation. Biomaterials 26(11):1211–1218.
Wu W, DeConinck A, Lewis JA. 2011. Omnidirectional printing of 3D microvascular networks. Adv Mater 23(24):H178–H183.
Xu T, Gregory CA, Molnar P, Cui X, Jalota S, Bhaduri SB, Boland T. 2006. Viability and electrophysiology of neural cell structures generated by the inkjet printing method. Biomaterials 27(19):3580–3588.
Xu F, Sridharan B, Wang SQ, Durmus NG, Shao L, Demirci U. 2011. Live sacrificial porogens for fabrication of porous hydrogel scaffolds. PLoS ONE 4:e19344.
Zawko SA, Schmidt CE. 2010. Crystal templating dendritic pore networks and fibrillar microstructure into hydrogels. Acta Biomaterialia 6(7):2415–2421.
Zhou LH, Huang GY, Wang SQ, Wu JY, Lee WG, Chen YM, Xu F, Lu TJ. 2011. Advances in cell-based biosensors using three-dimensional cell-encapsulating hydrogels. Biotechnol J 6(12):1466–1476.
Zhu JM. 2010. Bioactive modification of poly(ethylene glycol) hydrogels for tissue engineering. Biomaterials 31(17):4639–4656.